Int. J. of Thermal & Environmental Engineering
Volume 4, No. 1 (2012) 13-24

DTM- Padé Modeling of Natural Convective Boundary Layer Flow of a Nanofluid Past a Vertical Surface

M.M. Rashidi [a], O. Anwar Bég [b,*], M. Asadi [a], M.T. Rastegari [a]

[a] *Mechanical Engineering Department, Engineering Faculty of Bu-Ali Sina University, Hamedan, Iran*
[b] *Aerospace Engineering, Department of Engineering and Mathematics, Sheaf Building, Sheaf Street, Sheffield Hallam University, Sheffield, S11WB, England*

Abstract

In this paper, we study theoretically the natural convective boundary-layer flow of a nanofluid past a vertical plate. The model used for the nanofluid incorporates the effects of Brownian motion and thermophoresis. A similarity solution is developed. The similarity transformations are applied to reduce the governing partial differential equations to a set of nonlinear coupled ordinary differential equations in dimensionless form. A mathematical technique, namely the Differential Transform Method (DTM), is used to solve the nonlinear differential equations under appropriate boundary conditions, in the form of series with easily computable terms. Then, Padé approximants are applied to the solutions to increase the convergence of the given series. The combined DTM-Padé procedure is implemented directly without requiring linearization, discretization or perturbation. The solutions depend on a Lewis number (*Le*), a buoyancy-ratio number (*Nr*), a Brownian motion number (*Nb*), a thermophoresis number (*Nt*), as well as Prandtl number (*Pr*). Temperatures are shown to be enhanced with *Nb, Nr* and *Nt* increasing. Mass fraction function, *f*, is also reduced with increasing *Le*. The flow is accelerated with increasing *Pr*. The computations also indicate that the reduced Nusselt number is a decreasing function of each of *Nr, Nb* and *Nt*. Excellent correlation is also achieved between the DTM-Padé results and numerical shooting quadrature. The model has important applications in heat transfer enhancement in renewable energy systems and industrial thermal management.

Keywords: *Nanofluid; thermal convection; boundary layers; DTM-Padé solutions; Brownian motion; Lewis number; thermophoresis; convergence; heat transfer enhancement*

1. Introduction

The relatively poor heat transfer properties of common fluids (e.g. water, mineral oil and ethylene glycol arising in power generation, chemical processes and microelectronics, to name a few areas) compared to most solids is a major obstacle to the high compactness and effectiveness of heat exchangers. Nanofluids provide a significant improvement in the heat transfer properties of working fluids and hold immense potential in, for example, modern industrial energy processes and advanced nuclear systems as elaborated by Buongiorno and Hu [1]. The term ‘‘nanofluid‘‘ refers to a liquid containing a suspension of submicronic solid particles (nanoparticles) and was introduced by Choi [2]. The characteristic feature of nanofluids is thermal conductivity enhancement, a phenomenon observed by Masuda et al. [3]. Compared to suspended particles of millimeter-or-micrometer dimensions, nanofluids exhibit greater stability and rheological properties, dramatically higher thermal conductivities, and no penalty in pressure drop. Nanofluids are solid-liquid composite materials consisting of solid nanoparticles or nanofibers with sizes typically of 1-100 nm suspended in liquid. A small amount (<1% volume fraction) of Cu nanoparticles or carbon nanotubes dispersed in ethylene glycol or oil is reported to increase the inherently poor thermal conductivity of the liquid by 40% and 150%, respectively [4, 5]. Conventional particle-liquid suspensions require high concentrations (>10%) of particles to achieve such enhancement. However, problems of rheology and stability are amplified at high concentrations, precluding the widespread use of conventional slurries as heat transfer fluids. In some cases, the observed enhancement in thermal conductivity of nanofluids is orders of magnitude larger than predicted by well-established theories. A comprehensive survey of convective transport in nanofluids was made by Buongiorno [6], who developed a new model based on the mechanics of the nanoparticle base-fluid relative

* Corresponding author.
E-mail: o.beg@shu.ac.uk

DOI: 10.5383/ijtee.04.01.003

velocity, indicating that the nanoparticle absolute velocity can be viewed as the sum of the base fluid velocity and a relative velocity (termed "slip velocity"). This study has shown that the key phenomena dictating nanofluid thermal enhancement are Brownian diffusion and thermophoresis phenomena which are dominant contributors to heat transfer enhancement in nanofluids. Xuan and Li [7] presented an experimental study of convective heat transfer and flow features of the nanofluid in a tube, elucidating the influence of such factors as the volume fraction of suspended nanoparticles and the Reynolds number on the heat transfer and flow features and developing a novel convective heat transfer correlation for nanofluids. Boundary layer flows of nanofluids have also received some attention recently. Bachok et al [8] studied numerically the steady boundary-layer flow of a nanofluid past a moving semi-infinite flat plate in a uniform free stream with the plate able to translate in the same or opposite directions to the free stream. Khan and Pop [9] studied laminar boundary layer convection flow from a stretching flat surface in a nanofluid, showing that the reduced reduced Sherwood number is an increasing function of higher Prandtl number and a decreasing function of lower Prandtl number for each Lewis number, Brownian motion number or thermophoretic number. Nield and Kuznetsov [10] studied the free convection boundary layer flow in a nanofluid-saturated porous medium. Ahmad and Pop [11] examined the mixed convection nanofluid boundary layers along a vertical plane surface in a porous regime, for the case of different types of nanoparticles such as Cu (cuprom), Al2O3 (aluminium) and TiO2 (titanium).

In the present article we re-visit the nanofluid Pohlhausen–Kuiken–Bejan boundary layer problem using the model of Buongiorno [6], as first analyzed by Kuznetsov and Nield [12] who obtained a numerical solution. Owing to inherent nonlinearities in the reduced differential equations, no analytical solution is tractable and the nonlinear equations are invariably solved numerically subject to boundary conditions, one of which is prescribed at infinity. However with the rapid advancement of symbolic computation software such as MATHEMATICA, MATLAB etc, approximate analytic methods for nonlinear problems have been adopted by many researchers. Among these are the Homotopy Perturbation Method (HPM) [13] and Homotopy Analysis Method (HAM) [14]. Some of these methods use specific transformations in order to reduce the equations into simpler ones or system of equations and others yield the solution in a series form that converges to the accurate solution.

A robust semi-exact method which avoids the necessity for "small parameters" is the Differential Transform Method (DTM). The concept of DTM was first introduced by Zhou [15] for the solution of linear and non-linear initial value problems in electrical circuit theory applications. Chen and Ho [16] developed this method for partial differential equations. Ayaz [17] used DTM to study systems of differential equations. DTM is generally a powerful semi-analytical tool for engineering mechanics problems [18] and yields an analytical solution in the form of a polynomial. It is different from the traditional higher order Taylor series method. The traditional high order Taylor series method requires symbolic computation and is therefore a computationally intensive and expensive for large orders. Contrary to this, DTM obtains a polynomial series solution by means of an iterative procedure. DTM is therefore an alternative procedure for obtaining analytic Taylor series solution of the differential equations. With this method, it is possible to obtain highly accurate results or exact solutions for differential equations. In recent years, DTM has been successfully employed to solve many types of nonlinear problems in engineering science and applied physics including buckling of carbon nanotubes [19], water wave hydrodynamics [20], entropy generation in spinning disk flows [21], thermal design of fins [22], electrostatic imaging [23], diffusion-wave mechanics [24], thermal conduction [25], structural dynamics [26] and quantum mechanics [27]. All of these successful applications have rigorously verified the validity, effectiveness and flexibility of DTM.

DTM method constructs for differential equations an analytical solution in the form of a power series. Furthermore, power series are frequently inadequate for large values of say a space variable , as . It is now well known that Padé approximants [28, 29] have the advantage of manipulating the polynomial approximation into rational functions of polynomials. It is therefore essential to combination of the series solution, obtained by the DTM with the Padé approximant to provide an effective tool to handle boundary value problems at infinite domains. The first successful application of DTM to the boundary-layer flow equations was presented by Rashidi and Domairry [30]. Rashidi and Erfani [31] also demonstrated the applicability of DTM to thermal boundary-layer flow over a flat plate with convective surface boundary conditions. Herein, we generate a similarity model for free convection boundary-layer flow of a nanofluid past a vertical surface and implement the DTM method to obtain solutions for the transformed boundary layer problem.

2. Mathematical Model

Following Kuznetsov and Nield [12], we consider two-dimensional, steady, free convection boundary layer flow from a vertical surface, in an (x-y) coordinate system. The *x*-axis is aligned vertically upwards and the plate is located at $y = 0.$ At this boundary the temperature T and the nanoparticle fraction φ take constant values T_W and φ_W, respectively. The ambient values, attained as *y* tends to infinity, of T and φ are denoted by T_∞ and φ_∞, respectively. The Oberbeck–Boussinesq approximation is employed. The vectorial form of the conservation equations i.e. *mass, momentum, thermal energy, and nanoparticles*, respectively, in terms of the field variables (velocity v, the temperature T and the nanoparticle volume fraction $\varphi.$ is:

$$\nabla . v = 0, \tag{1}$$

$$\rho_f \left(\frac{\partial v}{\partial t} + v . \nabla v \right) = -\nabla p + \mu \nabla^2 v + \left[\phi \rho_p + (1-\phi) \{ \rho_f (1 - \beta (T - T_\infty)) \} \right] g, \tag{2}$$

$$(\rho c)_f \left(\frac{\partial T}{\partial t} + v . \nabla T \right) = k \nabla^2 T + (\rho c)_p [D_B \nabla \phi . \nabla T + (D_T / T_\infty) \nabla T . \nabla T], \tag{3}$$

$$\frac{\partial \phi}{\partial t} + v . \nabla \phi = D_B \nabla^2 \phi + (D_T / T_\infty) \nabla^2 T . \tag{4}$$

where ρ_f is the density of the base fluid and μ, k and β are respectively, the density, viscosity, thermal conductivity and volumetric volume expansion coefficient of the nanofluid, while ρ_p is the density of the particles, $v = (u, v).$ and gravitational acceleration is denoted by g. The coefficients that appear in Eqs. (3) and (4) are the *Brownian diffusion coefficient* (D_B) and the *thermophoretic diffusion coefficient* (D_T). Details of the derivation of Eqs. (3) and (4) are given in the papers by Buongiorno [6] and Nield and Kuznetsov [32] and Kuznetsov and Nield [33]. The boundary conditions are prescribed as follows:

$$u = 0, \quad v = 0, \quad T = T_W, \quad \phi = \phi_W \quad \text{at} \quad y = 0, \tag{5}$$

$$u = v = 0, \quad T \to T_\infty, \quad \phi \to \phi_\infty \quad \text{as} \quad y \to \infty. \tag{6}$$

In consistency with the Oberbeck–Boussinesq approximation and an assumption that the nanoparticle concentration is *dilute*, and with a suitable choice for the reference pressure, the momentum equation (2) may be linearized and written as follows [12]:

$$\rho_f\left(\frac{\partial v}{\partial t}+v.\nabla v\right)=-\nabla p+\mu\nabla^2 v+\left[\left(\rho_p-\rho_{f\infty}\right)(\phi-\phi_\infty)+(1-\phi_\infty)\rho_{f\infty}\beta(T-T_\infty)\right]g. \quad (7)$$

Employing the standard boundary-layer approximation, based on a scale analysis, the governing equations take the form:

$$\frac{\partial u}{\partial x}+\frac{\partial v}{\partial y}=0, \quad (8)$$

$$\frac{\partial p}{\partial x}=\mu\frac{\partial^2 u}{\partial y^2}-\rho_f\left(u\frac{\partial u}{\partial x}+v\frac{\partial u}{\partial y}\right)+\left[(1-\phi_\infty)\rho_{f\infty}\beta g(T-T_\infty)-(\rho_p-\rho_\infty)g(\phi-\phi_\infty)\right], \quad (9)$$

$$\frac{\partial p}{\partial y}=C, \quad (10)$$

$$u\frac{\partial T}{\partial x}+v\frac{\partial T}{\partial y}=\alpha\nabla^2 T+\tau\left[D_B\frac{\partial\phi}{\partial y}\frac{\partial T}{\partial y}+\left(\frac{D_T}{T_\infty}\frac{\partial T}{\partial y}\right)^2\right], \quad (11)$$

$$u\frac{\partial\phi}{\partial x}+v\frac{\partial\phi}{\partial y}=D_B\frac{\partial^2\phi}{\partial y^2}+\left(\frac{D_T}{T_\infty}\right)\frac{\partial^2 T}{\partial y^2}. \quad (12)$$

where:

$$\alpha=\frac{k}{(\rho c)_f}, \quad \tau=\frac{(\rho c)_p}{(\rho c)_f}. \quad (13)$$

The parameter p can be eliminated from Eqs. (9) and (10) by cross-differentiation. Furthermore we may introduce a stream function ψ defined by [12]:

$$u=\frac{\partial\psi}{\partial y}, \quad v=-\frac{\partial\psi}{\partial x}, \quad (14)$$

so that Eq. (8) is satisfied identically. The flow is then described with the following three equations:

$$\frac{\partial\psi}{\partial y}\frac{\partial^2\psi}{\partial x\partial y}+\frac{\partial\psi}{\partial x}\frac{\partial^2\psi}{\partial y^2}-\nu\frac{\partial^3\psi}{\partial y^3}=(1-\phi_\infty)\rho_{f\infty}\beta g(T-T_\infty)-(\rho_p-\rho_{f\infty})g\phi, \quad (15)$$

$$\frac{\partial\psi}{\partial y}\frac{\partial T}{\partial x}+\frac{\partial\psi}{\partial x}\frac{\partial T}{\partial y}=\alpha\nabla^2 T+\tau\left[D_B\frac{\partial\phi}{\partial y}\frac{\partial T}{\partial y}+\left(\frac{D_T}{T_\infty}\right)\left(\frac{\partial T}{\partial y}\right)\right], \quad (16)$$

$$\frac{\partial\psi}{\partial y}\frac{\partial\phi}{\partial x}+\frac{\partial\psi}{\partial x}\frac{\partial\phi}{\partial y}=D_B\frac{\partial^2\phi}{\partial y^2}+\left(\frac{D_T}{T_\infty}\right)\frac{\partial^2 T}{\partial y^2}. \quad (17)$$

In deriving Eq. (15), an integration with respect to y has been performed, and use has been made of the boundary conditions at infinity. Here $\nu=\mu/\rho_{f\infty}$. We now introduce the local Rayleigh number Ra_x defined by:

$$Ra_x=\frac{(1-\phi_\infty)\beta g(T_W-T_\infty)x^3}{\nu\alpha}, \quad (18)$$

and the similarity variable

$$\eta=\frac{y}{x}Ra_x^{1/4}. \quad (19)$$

The majority of industrial nanofluids [4, 5] possess high Lewis numbers; as such we restrict attention to the case of $Le>1$. In the regime studied the dominant driving force is due to *heat transfer* (and not *mass transfer*) which implies that the buoyancy-ratio parameter Nr defined by Eq. (25) below is much smaller than unity and the Lewis number Le defined by Eq. (28) is much greater than unity.

Proceeding with the analysis, the following dimensionless variables S, θ, and f are introduced:

$$S(\eta)=\frac{\psi}{\alpha Ra_x^{1/4}}, \quad \theta(\eta)=\frac{T-T_\infty}{T_W-T_\infty}, \quad f(\eta)=\frac{\phi-\phi_\infty}{\phi_W-\phi_\infty}. \quad (20)$$

Implementing these variables in Eqs. (15–17), readily yields the following *ordinary* differential equations:

$$S'''+\frac{1}{4\,\mathrm{Pr}}(3SS''-2S'^2)+\theta-Nr\,f=0, \quad (21)$$

$$\theta''+\frac{3}{4}S\theta'+Nbf'\theta'-Nt\theta'^2=0, \quad (22)$$

$$f''+\frac{3}{4}Le\,Sf'+\frac{Nt}{Nb}\theta''=0, \quad (23)$$

where the five thermophysical parameters are defined, as in [12] by:

$$\mathrm{Pr}=\frac{\nu}{\alpha}, \quad (24)$$

$$Nr=\frac{\left(\rho_p-\rho_{f\infty}\right)(\phi_W-\phi_\infty)}{\rho_{f\infty}\beta(T_W-T_\infty)(1-\phi_\infty)}, \quad (25)$$

$$Nb=\frac{(\rho c)_p D_B(\phi_W-\phi_\infty)}{(\rho c)_f\alpha}, \quad (26)$$

$$Nt=\frac{(\rho c)_p D_T(T_W-T_\infty)}{(\rho c)_f\alpha T_\infty}, \quad (27)$$

$$Le=\frac{\alpha}{D_B}. \quad (28)$$

Here Nr, Nb, Nt, Le denote a buoyancy ratio, a Brownian motion parameter, a thermophoresis parameter, and a Lewis number, respectively. The transformed two-point boundary value problem is highly nonlinear and coupled. The appropriate transformed boundary conditions are:

$$At\quad \eta=0:\quad S=0,\ S'=0,\ \theta=1,\ f=1. \quad (29)$$

$$As\quad \eta\to\infty:\quad S'=0,\ \theta=0,\ f=0. \quad (30)$$

When Nr, Nb and Nt vanish are all zero, Eqs. (21) and (22) involve just *two dependent variables*, namely S and θ, and the boundary-value problem for these two variables reduces to the classical *Pohlhausen–Kuiken–Bejan* problem. Of relevance to thermal engineering design (since we are primarily interested in heat transfer enhancement) is the Nusselt number, Nu which is formulated as:

$$Nu=\frac{q''x}{k(T_W-T_\infty)}, \quad (31)$$

where q'' is the wall heat flux. In the present context $Nu/Ra_x^{1/4}$ (referred to as the *reduced Nusselt number* and denote by Nur) is represented by $-\theta'(0)$.

3. Differential Transform Method (DTM) Analysis

Consider a function $u(x)$ which is analytic in a domain T and let $x=x_0$ represent any point in T. The function $u(x)$ is then represented by a power series whose centre is located at x_0. The differential transform of the function $u(x)$ is given by:

$$U(k)=\frac{1}{k!}\left[\frac{d^k u(k)}{dx^k}\right]_{x=x_0}, \quad (32)$$

where $u(x)$ is the original function and $U(k)$ the transformed function. The inverse transformation is defined as follows:

$$u(x)=\sum_{k=0}^{\infty}(x-x_0)^k U(k). \quad (33)$$

Inspection of Eq. (33), indicates that the concept of differential transform is derived from Taylor series expansion. However, this method does not evaluate the derivatives symbolically. In

actual applications, the function $u(x)$ is expressed by a *finite* series and Eq. (32) can be rewritten as follows:

$$u(x) \cong \sum_{k=0}^{m} (x - x_0)^k U(k). \tag{34}$$

which means that $u(x) = \sum_{k=m+1}^{\infty} (x - x_0)^k U(k)$ is negligibly small. Usually, the value of m is decided by convergence of the series coefficients. The operations for the *one–dimensional* differential transform method are provided in Table 1. Further details are provided in [30, 31].

4. Padé Approximants

Suppose that we are given a power series $\sum_{i=0}^{\infty} a_i x^i$, representing a function $f(x)$, such that:

$$f(x) = \sum_{i=0}^{\infty} a_i x^i. \tag{35}$$

The Padé approximant is a rational fraction and the notation for such a Padé approximant is [25, 26]

$$[L,M] = \frac{P_L(x)}{Q_M(x)}, \tag{36}$$

where $P_L(x)$ is a polynomial of degree at most L and $Q_M(x)$ is a polynomial of degree at most M. We have

$$f(x) = a_0 + a_1 x + a_2 x^2 + a_3 x^3 + a_4 x^4 + ..., \tag{37}$$

$$P_L(x) = p_0 + p_1 x + p_2 x^2 + p_3 x^3 + ... + P_L x^L, \tag{38}$$

$$Q_M(x) = q_0 + q_1 x + q_2 x^2 + q_3 x^3 + ... + q_M x^M, \tag{39}$$

We highlight that in Eq. (36) there are $L+1$ numerator coefficients and $M+1$ denominator coefficients. Since we can clearly multiply the numerator and denominator by a constant and leave $[L,M]$ unchanged, we impose the normalization condition:

$$Q_M(0) = 1. \tag{40}$$

So there are $L+1$ independent numerator coefficients and M independent denominator coefficients, making $L+M+1$ unknown coefficients in all. This number suggests that normally the $[L,M]$ ought to fit the power series Eq. (35) through the orders $1, x, x^2, ..., x^{L+M}$. Using the conclusion given in [25,26], we know that the $[L,M]$ approximant is uniquely determined. In the notation of formal power series:

$$\sum_{i=0}^{\infty} a_i x^i = \frac{p_0 + p_1 x + p_2 x^2 + ... p_L x^L}{q_0 + q_1 x + q_2 x^2 + ... + q_M x^M} + O(x^{L+M+1}). \tag{41}$$

By cross–multiplying Eq. (41), we find that

$$\begin{aligned}(a_0 + a_1 x + a_2 x^2 + a_3 x^3 + ...)(1 + q_1 x + q_2 x^2 + ... + q_M x^M) \\ = p_0 + p_1 x + p_2 x^2 + ... + p_L x^L + O(x^{L+M+1}).\end{aligned} \tag{42}$$

From Eq. (42), one can obtained the set of equations

$$\begin{cases} a_0 = p_0, \\ a_1 + a_0 q_1 = p_1, \\ a_2 + a_1 q_1 + a_0 q_2 = p_2, \\ \vdots \\ a_L + a_{L-1} q_1 + ... + a_0 q_L = p_L, \end{cases} \tag{43}$$

and

$$\begin{cases} a_{L+1} + a_L q_1 + ... + a_{L-M+1} q_M = 0, \\ a_{L+2} + a_{L+1} q_1 + ... + a_{L-M+2} q_M = 0, \\ \vdots \\ a_{L+M} + a_{L+M-1} q_1 + ... + a_L q_M = 0. \end{cases} \tag{44}$$

Where $a_n = 0$ for $n < 0$ and $q_j = 0$ for $j > M$.

If Eqs. (43) and (44) are nonsingular, then we can solve them directly

$$[L,M] = \frac{\begin{vmatrix} a_{L-M+2} & a_{L-M+2} & \cdots & \\ \vdots & \vdots & \ddots & \vdots \\ a_L & a_{L+1} & \cdots & \\ \sum_{j=M}^{L} a_{j-M} x^j & \sum_{j=M-1}^{L} a_{j-M+1} x^j & \cdots & \sum_{j=0}^{L} \end{vmatrix}}{\begin{vmatrix} a_{L-M+1} & a_{L-M+2} & \cdots & \\ \vdots & \vdots & \ddots & \vdots \\ a_L & a_{L+1} & \cdots & \\ x^M & x^{M-1} & \cdots & 1 \end{vmatrix}}. \tag{45}$$

If the lower index on a sum exceeds the upper, the sum is replaced by zero. Alternate forms are

$$\begin{aligned}[L,M] &= \sum_{j=0}^{L-M} a_j x^j + x^{L-M+1} w^T{}_{L/M} W^{-1}{}_{L/M} w_{L/M} \\ &= \sum_{j=0}^{L+n} a_j x^j + x^{L+n+1} w^T{}_{(L+M)/M} W^{-1}{}_{L/M} w_{(L+n)/M},\end{aligned} \tag{46}$$

for

$$W_{L,M} = \begin{bmatrix} a_{L-M+1} - x a_{L-M+2} & \cdots & -x a_{L+1} \\ \vdots & \ddots & \vdots \\ a_L - x a_{L+1} & \cdots & -x a_{L+M} \end{bmatrix} \tag{47}$$

$$w_{L,M} = \begin{bmatrix} a_{L-M+1} \\ a_{L-M+2} \\ \vdots \\ a_L \end{bmatrix} \tag{48}$$

The construction of $[L,M]$ approximants involves only algebraic operations [25,26]. Each choice of L, degree of the numerator and M, degree of the denominator, leads to an approximant. The major difficulty in applying the technique is how to direct the choice in order to obtain the best approximant. This needs the use of a criterion for the choice depending on the shape of the solution. We construct the approximants using Mathematica software in the following sections. More importantly, the diagonal approximant is the most accurate approximant; therefore we will construct only the diagonal approximants in the following discussions.

5. Analytical Approximations by the DTM–Padé Technique

The fundamental mathematical operations performed by **DTM** are listed in Table 1. Taking the differential transform of Eqs. (24) and (25), we obtain :

$$\begin{aligned}&(i+1)(i+2)(i+3)S[i+3] = Nr\ F[i] - \Theta[i] \\ &+2\left(1/(4\,\mathrm{Pr})\right) \sum_{k1=0}^{i} (S[k1+1](k1+1)(i+1-k1)S[i+1-k1]) - \\ &3\left(1/(4\,\mathrm{Pr})\right) \sum_{k2=0}^{i} (S[k2](i+2-k2)(i+1-k2)S[i+2-k2]),\end{aligned} \tag{49}$$

$$(i+1)(i+2)\Theta[i+2]=(-3/4)\sum_{k3=0}^{i}(S[k3](i+1-k3)\Theta[i+1-k3])$$
$$-Nt\sum_{k4=0}^{i}(\Theta[k4+1](k4+1)(i+1-k4)\Theta[i+1-k4]) \quad (50)$$
$$-Nb\sum_{k5=0}^{i}(\Theta[k5+1](k5+1)(i+1-k5)F[i+1-k5]),$$

$$(i+1)(i+2)F[i+2]=(-3/4)Le\sum_{k6=0}^{i}(S[k6](i+1-k6)F[i+1-k6]), \quad (51)$$
$$-(Nt/Nb)\Theta[i+2](i+1)(i+2)$$

where $S(i), \Theta(i)$ and $F(k)$ are the differential transform of $S(\eta), \theta(\eta)$ and $f(\eta)$ respectively. The transform of the boundary conditions are:

$$\begin{aligned} &S[0]=0, \quad S[1]=0, \quad S[2]=\Delta_1, \\ &\Theta[0]=1, \quad \Theta[1]=\Delta_2, \\ &F[0]=1, \quad F[1]=\Delta_3, \end{aligned} \quad (52)$$

where Δ_1, Δ_2 and Δ_3 are constants that are computed from the boundary condition. For computing their values, the problem is solved with initial condition (52) and then the boundary conditions (29) and (30) are applied. The simultaneous solution of the three resulting equations yields values for Δ_1, Δ_2 and Δ_3. For $Nb=Nr=Nt=0.5$ and $Le=\Pr=10$, we have found $\Delta_1=0.469481, \Delta_2=-0.2508571$ and $\Delta_3=-1.174326$. The ideal method for enlarging the convergence radius of the truncated series solution is the Padé approximant i.e. converting the polynomial approximation into a ratio of two polynomials. Without using the Padé approximant, the analytical solution obtained by the **DTM**, cannot satisfy boundary conditions at infinity. It is therefore essential to combine the series solution, obtained by **DTM** with the Padé approximant to provide an effective tool for accommodating boundary value problems in infinite domains.

6. Results and Discussion

An extensive range of computations has been performed with both numerical quadrature, **DTM** and **DTM-Padé** methods. The two-point boundary value problem for nanofluid boundary layer convection from a vertical surface is evidently governed by five independent dimensionless parameters, namely *Pr, Le, Nr, Nb, and Nt.* The far field boundary conditions must be applied in the computations at a finite value of the similarity variable, η, here denoted by $\eta_{\max}$. Bulk calculations were executed with the value $\eta_{\max}=10.$ In order to verify the accuracy of the present method, we have compared our results with those of numerical shooting method. The stream function, for **DTM**, **DTM–Padé** with various values of *L* and *M* (Padé parameters) and numerical quadrature are shown in Fig. 1. These results are given in Table 1. From Table 1 and Fig.1 we found that maximum difference between **DTM–Padé** [20, 21] and numerical quadrature is 0.00523 at $\eta=10$. The correlation is excellent between **DTM–Padé** and the numerical solutions; significant differences are however present with the much less accurate **DTM** method.

Table 1: The operations for the one–dimensional differential transform method

Original function	Transformed function
$w(x)=u(x)\pm v(x)$	$W(k)=U(k)\pm V(k)$
$w(x)=\lambda u(x)$	$W(k)=\lambda U(k), \lambda$ is a constant
$w(x)=x^r$	$W(k)=\delta(k-1)$, where $\delta(k-1)=\begin{cases}1, & \text{if } k=r\\ 0, & \text{if } k\neq r\end{cases}$
$w(x)=\dfrac{du(x)}{dx}$	$W(k)=(k+1)U(k+r)$
$w(x)=\dfrac{d^r u(x)}{dx^r}$	$W(k)=(k+1)(k+2)...(k+r)U(k+r)$
$w(x)=u(x)v(x)$	$W(k)=\sum_{r=0}^{k}U(r)V(k-r)$
$w(x)=\dfrac{du(x)}{dx}\dfrac{dv(x)}{dx}$	$W(k)=\sum_{r=0}^{k}(r+1)(k-r+1)U(r+1)V(k-r+1)$
$w(x)=u(x)\dfrac{dv(x)}{dx}$	$W(k)=\sum_{r=0}^{k}(k-r+1)U(r)V(k-r+1)$
$w(x)=u(x)\dfrac{dv(x)}{dx}\dfrac{dz(x)}{dx}$	$W(k)=\sum_{r=0}^{k}\sum_{t=0}^{k-r}(t+1)(k-r-t+1)\times U(r)V(t+1)Z(k-r-t+1)$

Table 2: $S(\eta)$ **obtained by the DTM, DTM–Padé and shooting (numerical) quadrature for** $Nb=Nr=Nt=0.5$ **and** $\Pr=Le=10.$

η	DTM	DTM–Padé [20,21]	DTM–Padé [21,22]	DTM–Padé [22,23]	DTM–Padé [23,24]	Numerical
0	0	0	0	0	0	0
2	1.29344	1.11664	1.11664	1.11664	1.11664	1.11664
4	7.52632E13	2.3808	2.38063	2.3807	2.3807	2.3808
6	1.62258E22	3.061	3.05555	3.05756	3.05752	3.061
8	1.2538E28	3.35615	3.33406	3.3428	3.34262	3.35647
10	4.56105E32	3.42952	3.38693	3.40583	3.40545	3.43043

Table 3: $\theta(\eta)$ **obtained by the DTM, DTM–Padé and its numerical values for** $Nb=Nr=Nt=0.5$ **and** $\Pr=Le=10.$

η	DTM	DTM–Padé [15,19]	DTM–Padé [18,23]	DTM–Padé [20,25]	DTM–Padé [22,27]	Numerical
0	1	1.00000	1.00000	1.00000	1.00000	1.00000
2	3291.67	0.27348	0.27348	0.27348	0.27348	0.27348
4	1.14988E18	0.01143	0.01086	0.01078	0.01248	0.01073
6	2.42418E26	0.00284	1.360E-7	-0.00147	0.00647	-0.00140
8	1.86018E32	0.00422	0.00054	-0.00159	0.00657	-0.00156
10	6.7457E36	0.00364	0.00048	-0.00161	0.00443	-0.00156

The temperature profile, $\theta(\eta)$ for **DTM**, **DTM–Padé** with various values of L and M (Padé parameters) and numerical shooting quadrature are shown in Fig. 2. These results are also given in Table 3. From Fig. 2 and Table 3 we found that maximum difference between **DTM–Padé** [20, 25] and numerical is 10^{-5}. The nanoparticle volume fraction, $f(\eta)$ for **DTM**, **DTM–Padé** with various values of L and M (Padé parameters) and numerical are shown in Fig. 3. These results are also given in Table 4.

Table 4: $f(\eta)$ obtained by the DTM, DTM–Padé and its numerical values for $Nb = Nr = Nt = 0.5$ and $\Pr = Le = 10$.

η	DTM	DTM–Padé [20,25]	DTM–Padé [22,27]	DTM–Padé [17,22]	DTM–Padé [18,25]	Numerical
0	1	1.00000	1.00000	1.00000	1.00000	1.00000
2	10486.	0.02679	0.02679	0.02679	0.02679	0.02679
4	3.76721E17	0.00092	0.00077	0.00252	0.00151	0.00118
6	2.93011E25	-0.00037	-0.00053	0.00060	0.00030	-0.00015
8	1.16606E31	-0.00017	-0.00025	0.00015	0.00022	-0.00017
10	2.58634E35	-0.00006	-0.00011	0.00004	0.00014	-0.00017

From Fig. 3 and Table 4 we found that maximum difference between DTM–Padé [20,25] and numerical solution is 10^{-4}.

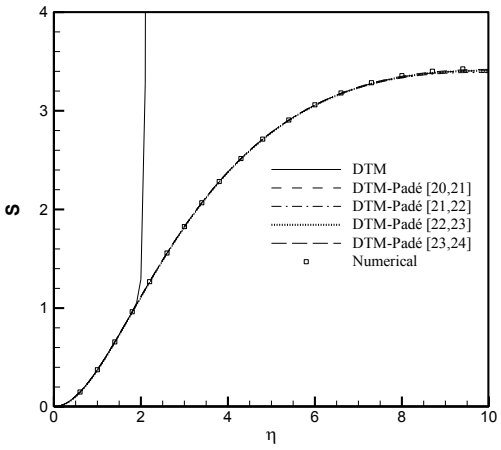

Figure 1: The behavior of the solutions S obtained by the DTM, DTM–Padé and numerical for $Nb = Nr = Nt = 0.5$ and $Le = \Pr = 10$.

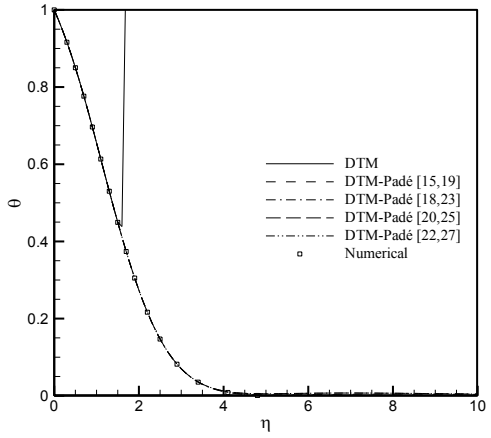

Figure 2: The behavior of the solutions θ obtained by the DTM, DTM–Padé and numerical quadrature for $Nb = Nr = Nt = 0.5$ and $Le = \Pr = 10$.

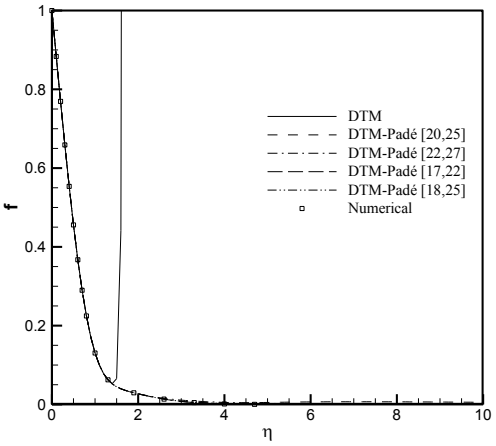

Figure 3: The behavior of the solutions f obtained by the DTM, DTM–Padé and numerical quadrature $Nb = Nr = Nt = 0.5$ and $Le = \Pr = 10$.

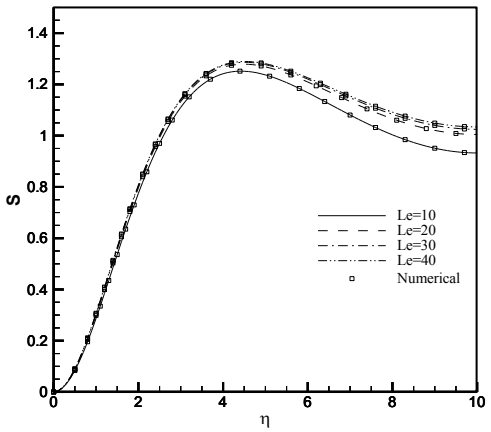

Figure 4: Effects of Lewis number (*Le*) on stream function, S obtained by the DTM, DTM–Padé and numerical quadrature with $Nb = Nr = Nt = 0.5$ and $\Pr = 1$.

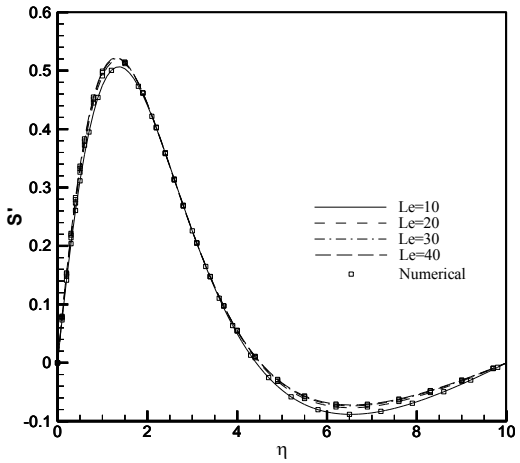

Figure 5: Effects of Lewis number (*Le*) on stream function gradient (velocity function), S' obtained by the DTM–Padé and numerical quadrature with $Nb = Nr = Nt = 0.5$ and $\Pr = 1$.

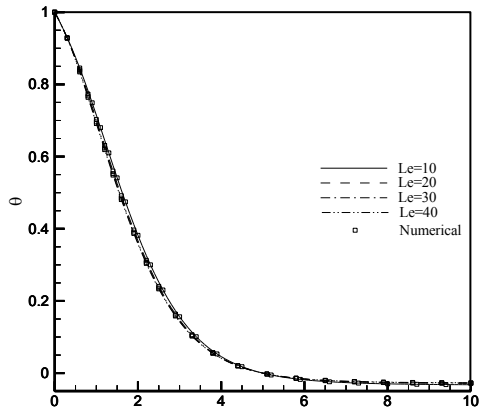

Figure 6: Effects of Lewis number (*Le*) on temperature function, θ obtained by the DTM–Padé and numerical quadrature with $Nb = Nr = Nt = 0.5$ and $\Pr = 1$.

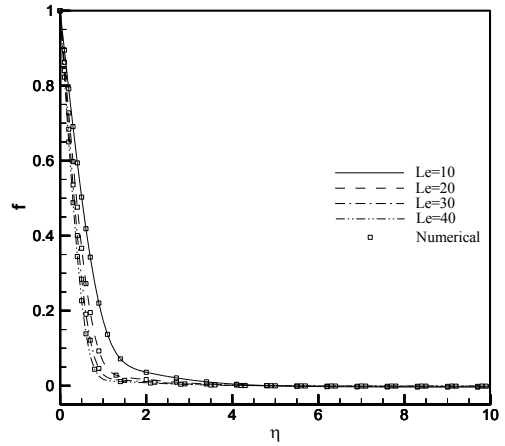

Figure 7: Effects of Lewis number (*Le*) on mass fraction function, f obtained by the DTM–Padé and numerical quadrature with $Nb = Nr = Nt = 0.5$ and $\Pr = 1$.

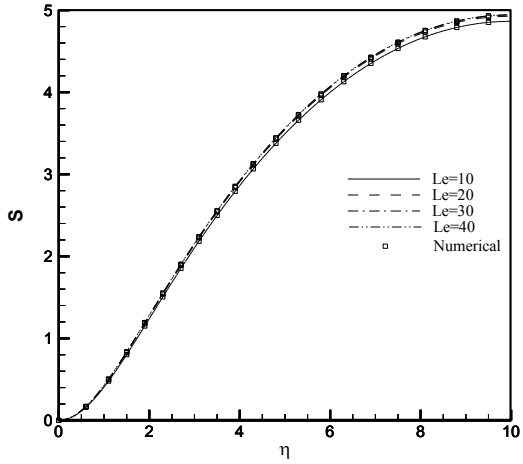

Figure 8: Effects of Lewis number (*Le*) on stream function, S obtained by the DTM–Padé and numerical quadrature with $Nb = Nr = Nt = 0.5$ and $\Pr = 100$.

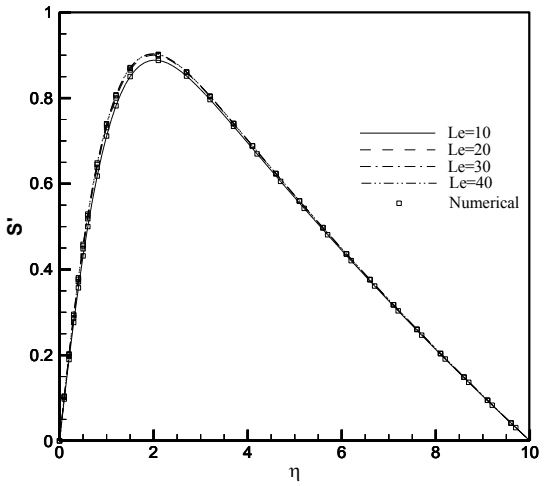

Figure 9: Effects of Lewis number (*Le*) on stream function gradient (velocity function) S' obtained by the DTM–Padé and numerical quadrature with $Nb = Nr = Nt = 0.5$ and $\Pr = 100$.

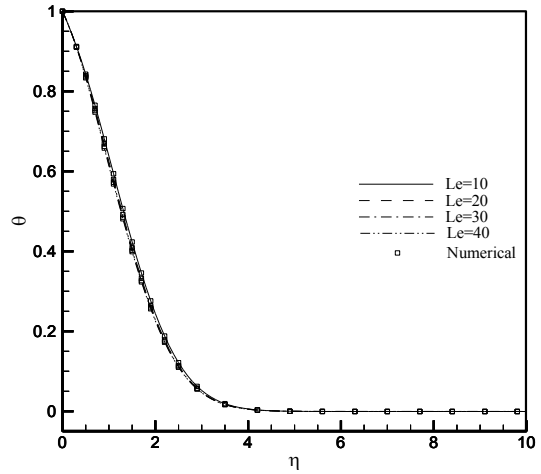

Figure 10: Effects of Lewis number (*Le*) on temperature function, θ obtained by the DTM–Padé and numerical quadrature with $Nb = Nr = Nt = 0.5$ and $\Pr = 100$.

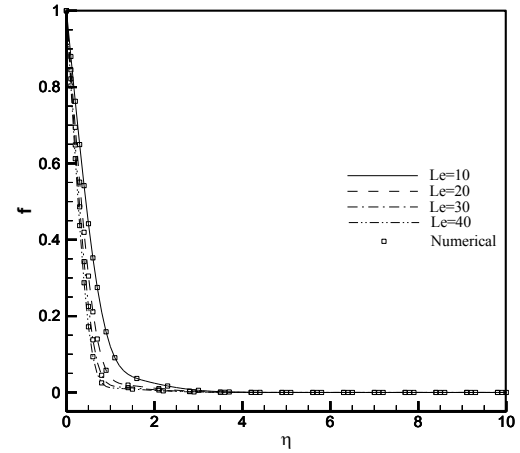

Figure 11: Effects of Lewis number (*Le*) on mass fraction function f obtained by the DTM–Padé and numerical quadrature with $Nb = Nr = Nt = 0.5$ and $\Pr = 100$.

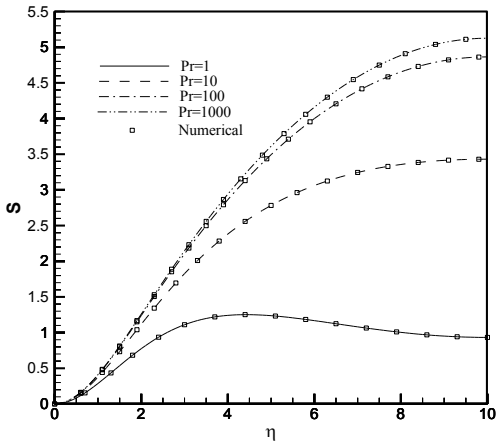

Figure 12: Effects of Prandtl number (*Pr*) on stream function, S obtained by the DTM–Padé and numerical quadrature with $Nb = Nr = Nt = 0.5$ and $Le = 10.$

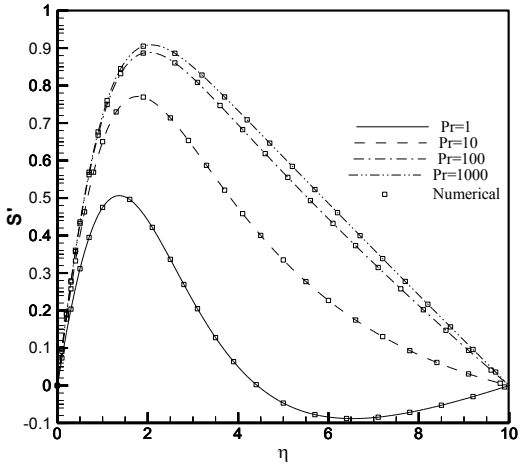

Figure 13: Effects of Prandtl number (*Pr*) on stream function gradient (velocity function), S' obtained by the DTM–Padé and numerical quadrature with $Nb = Nr = Nt = 0.5$ and $Le = 10.$

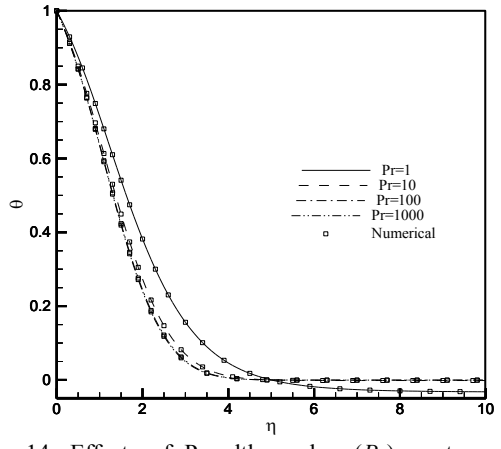

Figure 14: Effects of Prandtl number (*Pr*) on temperature function, θ obtained by the DTM–Padé and numerical quadrature with $Nb = Nr = Nt = 0.5$ and $Le = 10.$

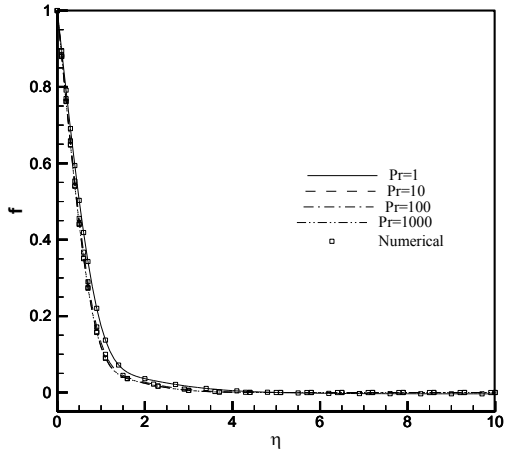

Figure 15: Effects of Prandtl number (*Pr*) on mass fraction function, f obtained by the DTM–Padé and numerical quadrature with $Nb = Nr = Nt = 0.5$ and $Le = 10.$

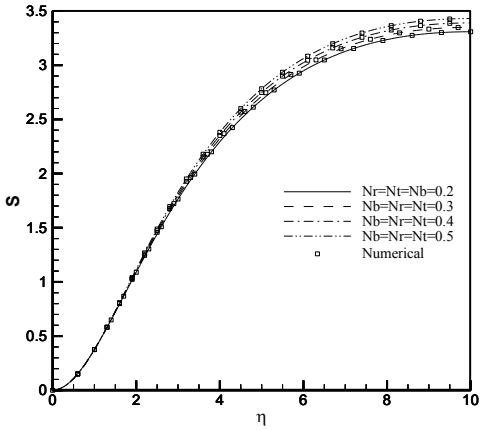

Figure 16: Combined effects of buoyancy ratio (*Nr*), Brownian motion parameter (*Nb*) and thermophoresis parameter (*Nt*) on stream function, S obtained by the DTM–Padé and numerical quadrature with $\Pr = 10$ and $Le = 10.$

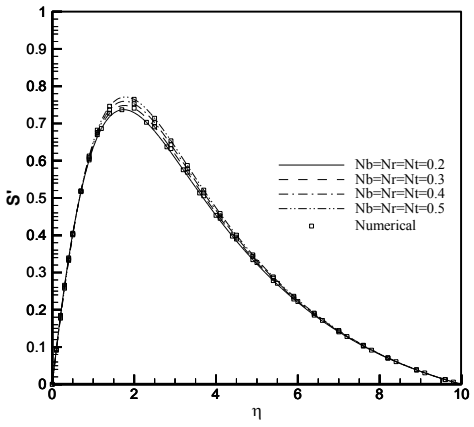

Figure 17: Combined effects of buoyancy ratio (*Nr*), Brownian motion parameter (*Nb*) and thermophoresis parameter (*Nt*) on stream function gradient (velocity function), S' obtained by the DTM–Padé and numerical quadrature with $\Pr = 10$ and $Le = 10.$

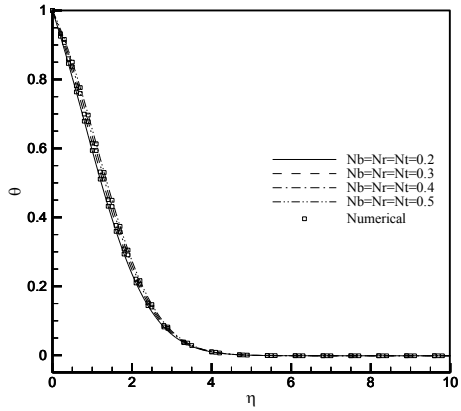

Figure 18: Combined effects of buoyancy ratio (*Nr*), Brownian motion parameter (*Nb*) and thermophoresis parameter (*Nt*) on temperature function, θ obtained by the DTM–Padé and numerical quadrature with $\Pr = 10$ and $Le = 10.$

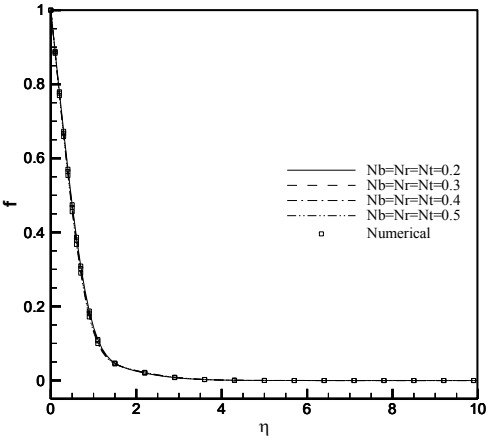

Figure 19: Combined effects of buoyancy ratio (*Nr*), Brownian motion parameter (*Nb*) and thermophoresis parameter (*Nt*) on mass fraction function, f obtained by the DTM–Padé and numerical quadrature with $\Pr = 10$ and $Le = 10.$

Figures 4 to 11 illustrate the influence of the Lewis number (*Le*) on the stream function (*S*), stream function gradient ($S^{/}$), temperature function (θ), and mass fraction function (*f*), for fixed values of the parameters Nr, Nb and Nt and *Pr*. **Lewis number** is a dimensionless number defined as the ratio of thermal diffusivity to mass diffusivity. It is used to characterize fluid flows where there is simultaneous heat and mass transfer by convection. *Le* expresses the ratio of the Schmidt number to the Prandtl number. For *Le* = 1, both heat and species will diffuse at the same rate. For *Le* < 1, heat will diffuse more slowly than species and vice versa for *Le* > 1. For the cases examined here, *Le* ≥ 10 i.e. thermal diffusion rate greatly exceeds the mass fraction (species) diffusion rate. Inspection of figure 6 shows that stream function (*S*) is clearly enhanced with an increase in *Le*. Close to the plate surface, stream function gradient i.e. velocity function (as shown in figure 5) is also enhanced with an increase in Le i.e. the flow is accelerated. However further from the plate surface i.e. with increasing η, all velocity profiles merge and only with subsequent distance from the plate does the Lewis number act to accelerate the flow again. With a rise in le from 10 through 20, 30 to 40, the temperature (figure 6) in the boundary layer regime is slightly reduced. The nanofluid regime is therefore cooled slightly with increasing Lewis number. Mass fraction function, *f*, is also reduced with increasing Lewis number (figure 7) and much more dramatically than temperature. *f* profiles are found to be very sharp decays from the plate surface whereas temperature profiles decay much more smoothly across the boundary layer. Figures 4 to 7 all correspond to *Pr = 1* i.e. where the momentum diffusivity and thermal diffusivity in the boundary layer are the same. Excellent correlation is achieved in all these graphs between DTM-Pade and numerical shooting solutions. Again In figures 8 to 11 we have computed the stream function (*S*), stream function gradient ($S^{/}$), temperature function (θ), and mass fraction function (*f*) distributions with various Lewis numbers, but for a much higher Prandtl number (= 100). Comparing figure 8 with figure 4 it is evident that for greater Prandtl number, the stream function is significantly boosted i.e. *S* values are considerably greater at the same values of Lewis number; also there is a montonic increase in *S* in figure 8 whereas the profiles in figure 4 peak at some distance from the plate surface and begin to decay. Comparing figure 9 with figure 5, we observe that there is also a greater magnitude of velocity i.e. stream function gradient, associated with *Pr* = 100, than for *Pr* = 1. The profiles in figure 5 exhibit a peak near the wall and a trough further from the wall; for figure 9 only a peak is observed, again close to the wall. Clearly, greater Prandtl number serves to accelerate the nanofluid boundary layer flow. Comparing the temperature distribution (figure 10) and mass fraction distribution (figure 11) for *Pr* = 100, with the respective graphs for *Pr* = 1 (i.e. figures 6 and 7 respectively), we observe that there is a very similar response with increasing Lewis number. Values of θ and *f* are however slightly lower for *Pr* = 100 than they are for *Pr* = 1.

A more detailed study of Prandtl number influence on the similarity functions, *S*, $S^{/}$, θ and *f*, is presented in **figures 12 to 15**. Stream function (figure 12) is observed to be strongly elevated with an increase in *Pr* from 1 through 10, 100 to 1000. Velocity function (i.e. $S^{/}$) as illustrated in figure 13, is also strongly enhanced with an increase in *Pr*. Temperature is however, as with conventional fluids, decreased markedly with an increase in *Pr*. *Pr* encapsulates the ratio of momentum diffusivity to thermal diffusivity for a given nanofluid implying that for lower *Pr* nanofluids, heat diffuses faster than momentum and vice versa for higher *Pr* fluids [34]. With an increase in Pr, temperatures will therefore fall i.e. the regime will be cooled as shown in figure 14. Mass fraction function (figure 14) is also reduced with increasing *Pr;* however the effect is less dramatic than for the temperature field. Larger *Pr* values correspond to a thinner thermal boundary layer thickness and more uniform temperature distributions across the boundary layer. Smaller *Pr* nanofluids possess higher thermal conductivities so that heat can diffuse away from the vertical plate faster than for higher *Pr* fluids (low *Pr* fluids correspond to thicker boundary layers). As such with an increase in *Pr*, momentum diffusivity will exceed thermal diffusivity and the nanofluid boundary layer flow will be accelerated as shown in figure 13. Again excellent correlation has been achieved between the DTM-Padé solutions and the numerical quadrature computations in each of the figures 12 to 15. More details of the DTM-Padé technique are discussed in Rashidi *et al.* [35].

In **figures 16 to 19**, the collective influence of buoyancy ratio (*Nr*), Brownian motion parameter (*Nb*) and thermophoresis parameter (*Nt*) on *S*, $S^{/}$, θ and *f*, with *Pr* = *Le* = 10 are illustrated. Clearly an increase in any of the buoyancy-ratio number *Nr*, the Brownian motion parameter *Nb*, or the

thermophoresis parameter *Nt* leads to an enhancement in the stream function (figure 16). Velocity in the boundary layer (figure 17) is also markedly enhanced with increasing *Nr, Nb* and *Nt* from 0.2, 0.3 through 0.4 to 0.5. Temperature is also evidently increased as *Nr, Nb* and *Nt increase*, as shown in figure 18. Very little alteration in mass fraction however is observed with a change in *Nr, Nb* and *Nt*. Although not computed, an increase in *Nr, Nb* and *Nt* will also serve to decrease the "reduced Nusselt number" which will correspond to an increase in the thermal boundary-layer thickness, owing to higher temperatures in the nanofluid regime. The nanofluid behaves more like a fluid than the conventional solid-fluid mixtures in which relatively larger particles with micrometer or millimeter orders are suspended [36, 37]. However the nanofluid is a two-phase fluid in nature and has some common features with solid-fluid mixtures. Random movement of the suspended nanoparticles *increases* energy exchange rates in the fluid. The dispersion will flatten temperature distribution and makes the temperature gradient between the fluid and wall (plate) steeper, which augments heat transfer rate between the fluid and the wall. The enhanced heat transfer by the nanofluid may result from either the fact that the suspended particles increase the thermal conductivity of the two-phase mixture or owing to chaotic movement of ultrafine particles accelerating energy exchange process in the fluid. Generally our computations concur with similar studies in the literature [8-11]. Overall the **DTM-Padé** approach again demonstrates very good correlation with the established numerical quadrature (shooting) method, and therefore provides a very useful benchmark for computational techniques such as finite differences [38], finite elements [39] and network electrical simulation methods [40].

7. Conclusions

In this paper, we have applied the **D**ifferential **T**ransform **M**ethod (**DTM**) to obtain approximate analytical solutions for incompressible, steady-state, free convective boundary-layer flow of a nanofluid past a vertical plate. The **DTM** approach combined with **Padé approximants** has been shown to be a promising tool to in solving two point boundary-value problems consisting of systems of nonlinear differential equations. The method has been applied directly without requiring linearization, discretization, or perturbation. The obtained results demonstrate the reliability of the algorithm and give it a wider applicability to nonlinear differential equations. Excellent correlation of the **DTM-Padé technique** with numerical quadrature (shooting solutions) has been demonstrated. We have examined the influence of nanoparticles on boundary-layer flow characteristics along a vertical plate, using a model in which Brownian motion and thermophoresis are accounted for. Effectively we have confirmed the trend of the results obtained by Kuznetsov and Nield [12], provided a robust alternative analytical methodology (which may serve as a verification tool to standard numerical methods) and also generalized the computations of [12] to consider a much wider variety of Lewis and Prandtl numbers. The present study has additionally served to verify that the reduced Nusselt number is lowered by increasing the nanofluid dynamic numbers Nr, Nb and Nt. and that temperatures in the nanofluid boundary layer are simultaneously increased with these parameters increasing. Presently the authors are applying the **DTM-Padé** technique to other complex multi-physical fluid dynamics problems including magnetohydrodynamic and rotating disk flows, the results of which will be communicated imminently.

Nomenclature

D_B	Brownian diffusion coefficient
D_T	thermophoretic diffusion coefficient
f	rescaled nanoparticle volume fraction, defined by Eq. (20)
g	gravitational acceleration vector
k	thermal conductivity
Le	Lewis number, defined by Eq. (28)
Nr	buoyancy-ratio parameter, defined by Eq. (25)
Nb	Brownian motion parameter, defined by Eq. (26)
Nt	thermophoresis parameter, defined by Eq. (27)
Nu	Nusselt number, defined by Eq. (31)
Nu_r	reduced Nusselt number, $Nu/Ra_x^{1/4}$
Pr	Prandtl number, defined by Eq. (24)
p	pressure
q''	wall heat flux
Ra_x	local Rayleigh number, defined by Eq. (18)
S	dimensionless stream function, defined by Eq. (20)
T	temperature
T_W	temperature at the vertical plate
T_∞	ambient temperature attained as y tends to infinity
v	velocity, (u,v)
(x,y)	Cartesian coordinates (x-axis is aligned vertically upwards, plate is at $y=0$)

Greek symbols

α	thermal diffusivity
β	volumetric expansion coefficient of the fluid
η	similarity variable, defined by Eq. (19)
θ	dimensionless temperature, defined by Eq. (20)
μ	dynamic viscosity of the fluid

ν kinematic viscosity, $\mu/\rho_{f\infty}$

ρ_f fluid density

ρ_p nanoparticle mass density

$(\rho c)_f$ heat capacity of the fluid

$(\rho c)_p$ effective heat capacity of nanoparticle

τ parameter defined by Eq. (13), $(\rho c)_p/(\rho c)_f$

φ nanoparticle volume fraction

φ_W nanoparticle volume fraction at vertical plate

φ_∞ ambient nanoparticle volume fraction attained as y tends to infinity

ψ stream function, defined by Eq. (14)

References

[1] J. Buongiorno, W. Hu, Nanofluid coolants for advanced nuclear power plants, Paper no. 5705, Proceedings of ICAPP '05, Seoul, South Korea, May 15-19 (2005).

[2] S. Choi, Enhancing thermal conductivity of fluids with nanoparticle, D.A. Siginer, H.P. Wang (Eds.), Developments and Applications of Non-Newtonian Flows, ASME, FED, **66**, 99-105 (1995).

[3] H. Masuda, A. Ebata, K. Teramae, N. Hishinuma, Alteration of thermal conductivity and viscosity of liquid by dispersing ultra-fine particles, Netsu Bussei, **7**, 227–233 (1993).

[4] J.A. Eastman, S.U.S. Choi, S. Li, W. Yu and L.J. Thompson, Anomalously increased effective thermal conductivities containing Copper nanoparticles, Applied Physics Letters, **78**, 718-720 (2001). doi:10.1063/1.1341218

[5] S.U.S. Choi, Z.G. Zhang, W. Yu, F.E. Lockwood, E.A. Grulke, Anomalous thermal conductivity enhancement on nanotube suspensions, Applied Physics Letters, **79**, 2252-2254 (2001). doi:10.1063/1.1408272

[6] J. Buongiorno, Convective transport in nanofluids, ASME J. Heat Transfer, **128**, 240 250 (2006).

[7] Y. Xuan and Q. Li, Investigation on convective heat transfer and flow features of nanofluids, ASME J. Heat Transfer, 125, 151-155 (2003). doi:10.1115/1.1532008

[8] N. Bachok, A. Ishak and I. Pop, Boundary-layer flow of nanofluids over a moving surface in a flowing fluid, Int. J. Thermal Sciences, **49**, 1663-1668 (2010). doi:10.1016/j.ijthermalsci.2010.01.026

[9] W.A. Khan and I. Pop, Boundary-layer flow of a nanofluid past a stretching sheet, Int. J. Heat and Mass Transfer, **53**, 2477-2483 (2010). doi:10.1016/j.ijheatmasstransfer.2010.01.032

[10] D.A. Nield and A.V. Kuznetsov, The Cheng-Minkowycz problem for natural convective boundary layer flow in a porous medium saturated by a nanofluid, Int. J. Heat and Mass Transfer, **52**, 5792-5795 (2009). doi:10.1016/j.ijheatmasstransfer.2009.07.024

[11] S. Ahmad and I. Pop, Mixed convection boundary layer flow from a vertical flat plate embedded in a porous medium filled with nanofluids, Int. Comm. Heat and Mass Transfer, **37**, 987-991 (2010). doi:10.1016/j.icheatmasstransfer.2010.06.004

[12] A.V. Kuznetsov and D.A. Nield, Natural convective boundary-layer flow of a nanofluid past a vertical plate, Int. J. Thermal Sciences, **49,** 243–247 (2010). doi:10.1016/j.ijthermalsci.2009.07.015

[13] J.H. He, Homotopy perturbation technique, Computer Methods in Applied Mechanics and Engineering, **178**, 257–62 (1999). doi:10.1016/S0045-7825(99)00018-3

[14] S.J. Liao, Beyond Perturbation: An Introduction to the Homotopy Analysis Method. Boca Raton, Chapman Hall/CRC Press, USA (2003). doi:10.1201/9780203491164

[15] J.K. Zhou, Differential Transformation and its Applications for Electrical Circuits, Huazhong Univ.Press, Wuhan, China (1986).

[16] C.K. Chen, S.H. Ho, Solving partial differential equations by two dimensional differential transform method, Applied Mathematics and Computation, **106**, 171–179 (1999). doi:10.1016/S0096-3003(98)10115-7

[17] F. Ayaz, Solutions of the systems of differential equations by differential transform method, Applied Mathematics and Computation, **147**, 547–567 (2004). doi:10.1016/S0096-3003(02)00794-4

[18] I.H. Abdel-Halim Hassan, Comparison differential transformation technique with Adomian decomposition method for linear and nonlinear initial value problems, Chaos Solitons & Fractals, **36**, 53–65 (2008). doi:10.1016/j.chaos.2006.06.040

[19] V. Senthilkumar, Buckling analysis of a single-walled carbon nanotube with nonlocal continuum elasticity by using differential transform method, Advanced Science Letters, **3**, 337-340 (2010).

[20] L. Zou, Z. Zong, Z. Wang and S. Tian, Differential transform method for solving solitary wave with discontinuity, Physics Letters A, **374**, 3451-3454 (2010). doi:10.1016/j.physleta.2010.06.066

[21] A. Arikoglu, G. Komurgoz, I. Ozkol and A. Y. Gunes, Combined effects of temperature and velocity jump on the heat transfer, fluid flow, and entropy

generation over a single rotating disk, ASME J. Heat Transfer, **132**, 34-43 (2010). doi:10.1115/1.4002098

[22] A.A. Joneidi, D.D. Ganji and M. Babaelahi, Differential Transformation Method to determine fin efficiency of convective straight fins with temperature dependent thermal conductivity, Int. Comm. Heat and Mass Transfer, **36**, 757-762 (2009). doi:10.1016/j.icheatmasstransfer.2009.03.020

[23] A. Ungar and H. C. Murrell, The differential transform and its application to an electrostatics image problem, Computers & Mathematics with Applications, **11**, 565-572 (1985). doi:10.1016/0898-1221(85)90038-0

[24] S. Momani, Z. Odibat, V. Ertürk, Generalized differential transform method for solving a space and time fractional diffusion-wave equation, Physics Letters A, **370**, 379-387 (2007). doi:10.1016/j.physleta.2007.05.083

[25] C. W. Bert, Application of differential transform method to heat conduction in tapered fins, ASME J. Heat Transfer, **124**, 208-209 (2002). doi:10.1115/1.1423316

[26] O. Ozdemir and M.O. Kaya, Flapwise bending vibration analysis of a rotating tapered cantilever Bernoulli-Euler beam by differential transform method, J. Sound and Vibration, **289**, 413-420 (2006). doi:10.1016/j.jsv.2005.01.055

[27] A.S.V. Ravi Kanth and K. Aruna, Two-dimensional differential transform method for solving linear and non-linear Schrödinger equations, Chaos, Solitons & Fractals, **41**, 2277-2281 (2009). doi:10.1016/j.chaos.2008.08.037

[28] G.A. Baker and P. Graves–Morris, Padé Approximants, Encyclopedia of Mathematics and its Application 13, Parts I and II:, Addison-Wesley Publishing Company, New York (1981).

[29] G.A. Baker, Essentials of Padé Approximants, Academic Press, London (1975).

[30] M.M. Rashidi, G. Domairry, New analytical solution of the three–dimensional Navier–Stokes equations, Modern Physics Letters B, **23**, 3147-3155 (2009). doi:10.1142/S0217984909021193

[31] M.M. Rashidi, E. Erfani, A Novel analytical solution of the thermal boundary–layer over a flat plate with a convective surface boundary condition using DTM–Padé, Int. Conference on Applied Physics and Mathematics (ICAPM 2009) 905–909 (2009).

[32] D.A. Nield, A.V. Kuznetsov, The onset of convection in a horizontal nanofluid layer of finite depth, European J. Mechanics - B/Fluids, **29**, 217-223 (2010). doi:10.1016/j.euromechflu.2010.02.003

[33] A. V. Kuznetsov and D. A. Nield, Thermal instability in a porous medium layer saturated by a nanofluid: Brinkman model, Transport in Porous Media, **81**, 409-422 (2010). doi:10.1007/s11242-009-9413-2

[34] H. Schlichting, Boundary-Layer Theory, 6th edition, MacGraw-Hill, New York (1979).

[35] M.M. Rashidi, N. Laraqi, S.M. Sadri, A novel analytical solution of mixed convection about an inclined flat plate embedded in a porous medium using the DTM-Padé, Int. J. Thermal Sciences, **49**, 2405-2412 (2010). doi:10.1016/j.ijthermalsci.2010.07.005

[36] M. Shafahi, V. Bianco, K. Vafai and O. Manca, An investigation of the thermal performance of cylindrical heat pipes using nanofluids, Int. J. Heat and Mass Transfer, **53**, 376-383 (2010). doi:10.1016/j.ijheatmasstransfer.2009.12.007; doi:10.1016/j.ijheatmasstransfer.2009.09.019

[37] S. Kakaç and A. Pramuanjaroenkij, Review of convective heat transfer enhancement with nanofluids, Int. J. Heat and Mass Transfer, **52**, 3187-3196 (2009). doi:10.1016/j.ijheatmasstransfer.2009.02.006

[38] A.S. Warke, S. K. Das, O. Anwar Bég, H. S. Takhar and T. A. Bég, Numerical modeling of transient mass transfer in an aquifer with simultaneous first order chemical reaction and second order decay using the **ADI** scheme, Int. J. Fluid Mechanics Research**, 35**, 2, 105-126 (2008). doi:10.1615/InterJFluidMechRes.v35.i2.20

[39] S. Rawat, R. Bhargava, R., Renu Bhargava and O. Anwar Bég, Transient magneto-micropolar free convection heat and mass transfer through a non-Darcy porous medium channel with variable thermal conductivity and heat source effects, Proc. IMechE Part C- J. Mechanical Engineering Science, **223**, 2341-2355 (2009).

[40] S.K. Ghosh, O. Anwar Bég, J. Zueco and Prasad, V. R., Transient hydromagnetic flow in a rotating channel permeated by an inclined magnetic field with magnetic induction and Maxwell displacement current effects, ZAMP: J. Applied Mathematics and Physics, **61**, 147-169 (2010). doi:10.1007/s00033-009-0006-2